Transport in rough self-affine fractures

German Drazer* and Joel Koplik†
Benjamin Levich Institute and Department of Physics, City College of the City University of New York, New York, New York 10031
(Received 10 October 2001; revised manuscript received 16 May 2002; published 15 August 2002)

Transport properties of three-dimensional self-affine rough fractures are studied by means of an effective-medium analysis and numerical simulations using the Lattice-Boltzmann method. The numerical results show that the effective-medium approximation predicts the right scaling behavior of the permeability and of the velocity fluctuations, in terms of the aperture of the fracture, the roughness exponent, and the characteristic length of the fracture surfaces, in the limit of small separation between surfaces. The permeability of the fractures is also investigated as a function of the normal and lateral relative displacements between surfaces, and it is shown that it can be bounded by the permeability of two-dimensional fractures. The development of channel-like structures in the velocity field is also numerically investigated for different relative displacements between surfaces. Finally, the dispersion of tracer particles in the velocity field of the fractures is investigated by analytic and numerical methods. The asymptotic dominant role of the geometric dispersion, due to velocity fluctuations and their spatial correlations, is shown in the limit of very small separation between fracture surfaces.

DOI: 10.1103/PhysRevE.66.026303 PACS number(s): 47.11.+j, 47.55.Mh, 02.50.−r, 05.40.−a

I. INTRODUCTION

The transport of fluids in geological media plays a dominant role in different applications such as subsurface hydrology, hydrocarbon recovery, and waste storage, and the transport properties of such media involves a combination of fluid flow at different length scales. First, there is transport at the microscopic level through the pore space of the rock itself. Then, at macroscopic length scales, the flow through fractures is, in most cases, the dominant transport mechanism. Finally, at even larger length scales, the dominant convective transport involves the flow through fracture networks. The first case has received considerable attention and is relatively well understood and, in fact, it can be placed within the framework of transport in porous media [1–3]. On the other hand, understanding the flow through single fractures is clearly a prerequisite to the investigation or modeling of more complex cases such as the flow through macroscopic fracture networks. Another key transport process present in geological systems, the transport of tracer particles carried by the fluid also requires an adequate understanding of the flow properties, in particular, the statistical properties of the velocity field.

Fractures have often been modeled as simple Hele-Shaw cells, with a cubic relation between the volumetric flow rate and the average aperture of the fracture, usually focusing most of the effort on investigating the flow through a macroscopic network of such fractures. However, although a typical fractured rock surface appears fairly smooth, aside from some random roughness, suggesting that Poiseuille flow in a straight channel is the appropriate model of flow, laboratory experiments [4,5] and numerical simulations [6,7] indicate that this classical view of a rock fracture as a straight channel is not adequate to describe the fluid flow even at low Reynolds numbers. In fact, more careful analysis showed, in recent years, that geological fractures present highly spatially correlated, self-affine surfaces, with a roughness exponent $\zeta \approx 0.8$ surprisingly constant for different types of rocks whether naturally or artificially fractured [5,8–11]. In view of these results, theoretical and numerical studies introduced the complex geometry of the fractures in order to calculate the transport properties of the system. However, the majority of these studies assumed that the Reynolds (lubrication) approximation is valid so that the velocity field is given by a Poiseuille flow everywhere, with a parabolic velocity profile across the aperture and in the direction of the mean flow [6,11–17]. While this approximation has proven very useful in the case of uncorrelated opposing fracture surfaces (fracture *faults*) [11,17], it clearly fails to capture the roughness effects in the case we consider here—perfectly mated fracture surfaces in which the aperture is constant (fracture *joints*). In the lubrication approximation, our rough fractures are equivalent to a channel with a constant-width gap, without the vertical components of the fluid velocity which are particularly important in the limit of narrow fractures where the roughness amplitude is large compared to the aperture.

In a previous work [7], we proposed a different approach in which a two-dimensional fracture is divided into approximately straight segments with varying orientation angles. This approach allowed us to obtain the correction to the flow rate due to surface roughness as a function of the aperture and was validated by our numerical simulations. (A similar approach was used by Oron and Berkowitz to analyze the case of fractures with contacts between surfaces [18].) In this work, we shall further investigate the case of narrow fractures, extending the results to three-dimensional fractures. We shall see that it is possible to obtain analytic expressions for the permeability of the fracture and for the velocity fluctuations, in the limit of narrow fractures, by means of the effective-medium approximation. We shall also investigate the dispersion of tracer particles advected by the flow field

*Electronic address: drazer@mailaps.org
†Electronic address: koplik@sci.ccny.cuny.edu

within the fracture and its dependence on the aperture.

We shall first, in Sec. II, briefly discuss some basic definitions associated with self-affine surfaces and present our model of fractures as the gap between two perfectly matching self-affine surfaces. The Lattice-Boltzmann method, used to numerically simulate the fluid flow through the fractures, is briefly presented in Sec. III. Then, in Sec. IV we shall investigate the permeability by means of the effective-medium approximation and compare the results with our numerical results. Finally, in Sec. V we investigate the dispersion of tracer particles convected by the flow field within the fracture and its dependence on the aperture of the fracture.

II. SELF-AFFINE FRACTURE SURFACES

Following the work of Mandelbrot [19], the application of the fractal model to describe surface topography has become widespread as it has been shown in several experiments that fracture surfaces, with various materials and fracturing methods, exhibit statistically self-affine scaling properties. Particularly relevant to our work are the experiments performed with naturally fractured rocks [20–23]. This self-affine description of fracture surfaces substantially improves the characterization of rough surfaces in terms of surface mean parameters such as the root-mean-square (rms) roughness, rms slope, and density of peaks, in that it provides the scaling behavior of these parameters, which are not intrinsic properties of the surface but strongly depend on the sample size [20,21].

We consider a rock surface without overhangs [20], whose height is given by a single-valued function $z(x,y)$, with the coordinates x and y lying in the mean plane of the fracture. Self-affine surfaces display scale invariance with different dilation ratios along different spatial directions. Here we consider disordered media, so these scaling laws apply only in an ensemble or spatial average sense. Experiment indicates that for many materials isotropy can be assumed in the mean plane. Therefore, the surface height is a homogeneous function, of degree ζ, on the mean plane coordinates [24],

$$z(x,y)=\lambda^{-\zeta}z(\lambda x,\lambda y), \tag{1}$$

where ζ is usually referred to as the roughness or Hurst exponent [19].

In studies with several different types of fractured rocks the roughness exponent is found to be close to $\zeta=0.8$, independent of the material and of the fracture mode [5,8–11,21,22].

The Hurst exponent is not enough to describe a self-affine surface, and, in addition, the amplitude of the fluctuations in the height of the surface is to be specified. This amplitude of the fluctuations is usually expressed in terms of the characteristic length ℓ, which is the horizontal distance over which fluctuations in height have a rms slope of one, $\sigma_z^2(\ell)=\ell^2$. Using the self-affine scaling law we can then obtain the variance of the fluctuations in surface height, over any length scale r, in terms of the roughness exponent ζ and the characteristic length ℓ,

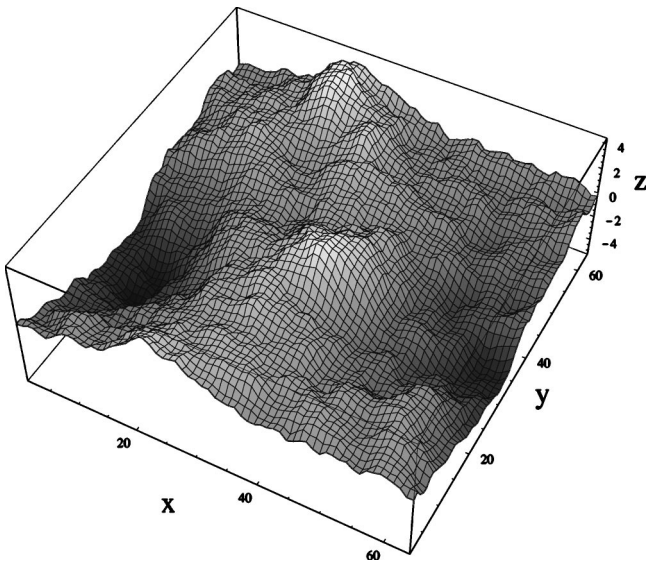

FIG. 1. Example of a numerically generated self-affine surface, with roughness exponent $\zeta=0.8$, characteristic length $\ell\simeq 3\times 10^{-3}$, and size $L\times L=64\times 64$.

$$\sigma_z^2(r)=\langle[z(\overline{r'})-z(\overline{r'}+\overline{r})]^2\rangle=\ell^2\left(\frac{r}{\ell}\right)^{2\zeta}. \tag{2}$$

In principle, the characteristic length ℓ can take any value, however, for fractured rocks it is usually found to be very small, and to lie either below the accessible range of length scales in the experiment ($\ell\leqslant 0.5\ \mu$m [21]) or below the self-affine range of the surface [5,25]. Therefore, we shall not consider cases in which ℓ is within the simulated range of length scales.

The self-affine surfaces are generated by a two-dimensional generalization of the Fourier synthesis method previously used by us for the generation of self-affine curves [7]. Initially, an $L\times L$ matrix, where each element will represent the height of the discrete version of the fracture surface, is generated with statistically independent, Gaussian distributed, random numbers. Then, the Fourier transform of this initial random matrix is modulated by a power-law high-wave-numbers filter that introduces height-to-height correlations [26]. Finally, the whole surface is rescaled in order to get the desired characteristic length ℓ. In this work we shall use $\zeta=0.8$ and $\ell\simeq 3\times 10^{-3}$. This numerical method generates homogeneous and isotropic surfaces, and is preferable instead of other numerical methods such as the random addition algorithm (for a discussion of this point see Ref. [27], Sec. V A). The surfaces generated are periodic in x and y, as is shown in Fig. 1, and, although the periodicity is not physically important it has some computational advantages when calculating the flow field using periodic boundary conditions.

We shall model fractures as the gap between a self-affine surface and its replica, which is translated by a fixed distance h in the direction normal to the mean plane of the surface. However, during the fracturing process of the rock, the opposite matching surfaces might experience a lateral shift, in addition to the vertical displacement. Therefore, we shall

also consider this situation by introducing a lateral shift to the upper surface either along the direction of the mean flow or perpendicular to it.

In this work, we will analyze, for both types of fractures, with and without lateral shift, the case of *narrow fractures*, in which the gap size h is small compared to the vertical fluctuations of the fracture surface over length scales comparable to the size of the system L. In view of Eq. (2), we obtain that fluctuations of the surface height over the whole system are given by $\sigma_z(L)=\ell(L/\ell)^{\zeta}$ and, then the limiting situation of narrow fractures corresponds to, $(h/\ell)\ll(L/\ell)^{\zeta}$. In our simulations, for systems size $L=512$ the largest gap size consistent with the previous constraint is $h_{max}\sim 50$. In our numerical simulations, unless otherwise stated, we use ten statistically independent realizations of the fracture surface, and the results presented correspond to the average over these different realizations.

III. LATTICE-BOLTZMANN METHOD

The Lattice-Boltzmann method (LBM) [28,29] is particularly suitable to investigate the flow of fluids in highly irregular geometries, and, specifically, to study the various features of transport in self-affine rough fractures which are sensitive to their complex geometrical structure. A brief description of this algorithm is presented in our previous work [7]. Periodic boundary conditions are used for the inflow and outflow surfaces and a constant pressure gradient forcing the fluid is added in the x direction, while the gap between surfaces extends over z.

In what follows all quantities will be rendered dimensionless by the characteristic units of the numerical simulation. That is, taking the lattice spacing as the unit length and the simulation time step as the time unit. Note that, since we are concerned with incompressible flows, we do not need to introduce a dimension of mass. The relaxation time is chosen so that the kinematic viscosity is $\nu=0.1$ in dimensionless units. The pressure gradient is $\nabla p=6.25\times10^{-6}$, yielding a mean velocity in the range $2.0\times10^{-4}<U_x<2.0\times10^{-2}$, for separation between surfaces of the fracture between $8\leqslant\leqslant 64$. Then, for apertures h not larger than $h_S=20$, the Reynolds number is $\mathrm{Re}=U_x h/\nu<1$ and the flow is governed by the linear Stokes equations, which are invariant under velocity rescaling. Moreover, using the results of Ref. [30], where inertia effects in a self-affine channel are investigated, we see that for apertures $h=32$ ($\mathrm{Re}=1.6$; note the porosity factor in Ref. [30]), the deviation from the Stokes result for the pressure loss is less than 0.78%. Therefore, possibly aside from the simulations with the largest aperture $h=64$, there are no significant inertia effects on the flow rate.

IV. PERMEABILITY OF SELF-AFFINE FRACTURES

Let us consider first the case in which the two matching surfaces of a fractured rock are separated by a distance h in the normal direction, with no lateral shift between them. In this situation, the aperture of the fracture is clearly constant everywhere, but the effective local aperture for fluid flow, i.e., the local width of the fracture channel normal to the mean flow direction strongly depends on the local angle between the surface and its mean plane. The following theoretical analysis will be based on a kind of local lubrication approximation, in which the fracture is divided into smaller rectangular blocks. The linear size ξ of the blocks will be estimated as the length scale over which fluctuations in the surface height are small compared to the aperture and thus, each of these basic blocks can be considered, approximately, as two facing planes separated a distance h and with varying orientation angles with respect to the mean plane of the fracture.

A. Analog resistor network and effective-medium approximation

The transport properties of these narrow fractures can be modeled using effective-medium ideas. The representation of the fracture in terms of quasilinear blocks with random orientation can be mapped onto a regular two-dimensional square lattice, of lattice spacing ξ, where the disorder only enters the distribution of hydraulic conductances lying on each of the lattice bonds. Moreover, fluid flow is a locally conserved quantity at the lattice nodes and therefore this representation of the fracture is completely analogous to the classical random resistor networks that model electrical transport in disordered media [31,32,34]. This electrical analog, in combination with the Reynolds approximation, has been used previously in somewhat related contexts—to describe the flow behavior of fracture faults and the dependence of the permeability on the contact area between opposite surfaces [12,13], and to calculate the conductivity of fracture faults as a function of the separation between uncorrelated opposite fracture surfaces [14,33].

Consider the two opposite ends a and b of a single quasilinear block of a fracture, and its representation by a conductance joining the corresponding two lattice nodes a and b. Moreover, consider that a pressure drop is imposed between the two nodes, and that the lattice bond joining a and b is oriented either parallel or perpendicular to the mean flow. Using the Poiseuille result for the flow through this segment of the fracture we have that

$$Q_{a\to b}=-\frac{[h\cos(\theta)]^3}{12\mu}\frac{\Delta p_{ab}}{[\xi/\cos(\theta)]}=-g_{ab}\Delta p_{ab}, \quad (3)$$

where $Q_{a\to b}$ is the flow rate from node a to node b, g_{ab} is the bond conductance, ξ is the linear size of the block, and θ is the orientation angle of the block, with respect to the mean plane of the fracture, in the direction of the imposed pressure drop Δp_{ab}. Let us note that a slightly different approximation to the transport of fluid in a single block can be made by modeling each block as a cylinder of diameter $h\cos(\theta)$ and length ξ. However, these two approximations will only differ by a numerical factor, given that the ratio of the permeability of a cylinder to that of two parallel planes is independent of the separation between surfaces, $k_{straight}/k_{cylinder}=32/12$.

Furthermore, the fluid is incompressible and flux is conserved at each lattice node,

$$\sum_{a\to b} g_{ab}(p_a - p_b) = 0, \tag{4}$$

where the sum is over all nodes a connected directly to b. Then, the problem is now to solve the previous system of equations in the case where the hydrodynamic conductances g_{ab} vary according to some probability distribution, and we shall discuss now an approximation commonly used to solve this type of problems in the physics of disordered media, namely, the *effective-medium theory*.

The effective-medium approximation (EMA) is a standard method commonly used to calculate effective properties of a microscopically disordered medium, in which the random microscopic parameters are replaced by a certain mean value, chosen in a self-consistent way (a detailed discussion of this approximation can be found elsewhere [31,35]). The idea then is to choose a mean EMA hydraulic conductance g_m, in a self-consistent way, such that it reproduces the average local field. That is, the criterion to choose g_m within EMA is to require that the extra pressure differences, δp_{ab} induced when one individual conductance reverts from g_m to its original value g_{ab} average to zero [36],

$$\left\langle \frac{g_m - g}{g_m + g} \right\rangle = 0. \tag{5}$$

B. Probability distribution of conductances and mean EMA conductance

In order to determine the mean EMA conductance g_m, we first need to obtain the probability distribution of the individual bond conductances g_{ab}. The conductance of a single block is determined by the angle between the local orientation of the surface and the mean plane of the fracture [see Eq. (3)]. In terms of the height difference Z between the two ends of the block, the bond conductance can be written as

$$g(Z) = G_0 \left(\frac{\xi^2}{\xi^2 + Z^2} \right)^2, \quad G_0 = \frac{h^3}{12\mu\xi}. \tag{6}$$

Then, the average over local conductances given in Eq. (5) can be performed in terms of the distribution of height differences Z, between points of the fracture surface separated by a distance ξ (note that ξ is the distance between two points lying on the fracture surface projected over the mean plane, i.e., the lattice constant.)

Experimental measurements indicate that the distribution of heights, $p(Z)$, can be accurately described by a Gaussian distribution, at least for low-order moments [9,37]. Guided by these results, the numerical procedure used to generate the fracture surfaces is intended to produce self-affine surfaces with Gaussian fluctuations of the height, as discussed in Sec. II. Moreover, the perturbative analysis we shall present shows that higher moments of the height distribution function are related to higher order corrections to g_m and, therefore, the exact functional form of the distribution is not relevant but only its low-order moments.

Finally, we assume that neighboring conductances are uncorrelated. Note that short-range order induced by the correlated topography of the fracture surfaces is accounted for by means of the distribution of possible local orientation angles of the unit blocks. In a similar manner in Ref. [14], short-range correlations were included by fixing the topology of the fundamental unit to be either *hats* or *buckets*, representing peaks and valleys of the fracture surface (see Sec. 2.2 in Ref. [14]). Moreover, although long-range correlations are not explicitly included in the effective-medium approximation, it has been shown that EMA accurately describes the effective conductivity of two-dimensional networks close to the percolation threshold [33]. On the other hand, effective-medium is a poor approximation in the presence of long-range spatial correlations, as arise in the presence of flow *channeling* [14] or heterogeneities at the fracture scale [11,17], found in the case of uncorrelated opposing fracture surfaces. Assuming then a random distribution of local conductances, we can rewrite the integral equation (5), which defines the EMA conductance g_m, in terms of the reduced variable $x = Z/\sigma_z(\xi)$, which is normally distributed,

$$\int dx \frac{1}{\sqrt{2\pi}} \exp\left(-\frac{x^2}{2} \right) \frac{g_m(1+\epsilon^2 x^2)^2 - G_0}{g_m(1+\epsilon^2 x^2)^2 + G_0} = 0, \tag{7}$$

where the dimensionless parameter $\epsilon = \sigma_z(\xi)/\xi$ is the ratio between the average magnitude of the fluctuations in the height of the surface $\sigma_z(\xi)$ over a single block, and the size of these blocks ξ. In general, if the individual blocks of the fracture are smaller than the characteristic length $\xi < \ell$ we have that $\epsilon > 1$, and $\epsilon < 1$ for ξ larger than ℓ. However, since we consider the case in which the characteristic length is small compared to the simulated length scales ($\ell \sim 10^{-3} \ll 1$, see Sec. II), we have that

$$\epsilon \equiv \frac{\sigma_z(\xi)}{\xi} = \left(\frac{\xi}{\ell} \right)^{\zeta - 1} \ll 1. \tag{8}$$

Therefore, we can then evaluate the mean EMA conductance in a perturbative weak-disorder expansion by computing successive terms in the series expansion of g_m in the perturbative parameter ϵ,

$$g_m = g_m^0 + g_m^1 \epsilon^2 + g_m^2 \epsilon^4 + \cdots. \tag{9}$$

Replacing this series expansion of g_m into Eq. (7), rearranging terms by their order in ϵ, and given that the equation must be satisfied for any value of ϵ, we obtain the following expressions for g_m^i:

$$g_m^0 = G_0, \tag{10a}$$

$$g_m^1 = -2\langle x^2 \rangle G_0, \tag{10b}$$

$$g_m^2 = [\langle x^4 \rangle + 2\langle x^2 \rangle^2] G_0. \tag{10c}$$

Finally, computing the second and fourth moments of the Gaussian distribution, we obtain the expansion in power series of ϵ for the mean EMA conductance,

$$g_m = G_0[1 - 2\epsilon^2 + 5\epsilon^4 + O(\epsilon^6)]. \tag{11}$$

Let us remark that only the second and fourth moments of the Gaussian probability distribution of heights were involved in the previous calculation, and higher moments only occur in higher order terms, $O(\epsilon^6)$. On the other hand, to compute higher order terms in the ϵ expansion of the electrical conductivity of the network would require a different approach, e.g., a perturbative weak-disorder expansion of the conductivity in terms of the moments of the probability distribution of bond conductances to directly solve Eq. (4), since EMA would no longer be an accurate approximation [38].

The previous result for the mean EMA conductance g_m shows an important feature of the fractures, in that the same result, up to second order in ϵ, is obtained if those conductances that are perpendicular to the mean flow are eliminated from the resistor network, i.e., it predicts a *quasi-one-dimensional* flow. The two-dimensional character of the network only affects higher order terms, $O(\epsilon^4)$. In fact, deriving from the previous equation the permeability of the fracture we obtain,

$$k \approx \frac{h^2}{12}\left[1 - 2\left(\frac{\sigma_z(\xi)}{\xi}\right)^2\right], \tag{12}$$

which is the same result as obtained in Ref. [7] for two-dimensional fractures [see Eq. (29) in Ref. [7]].

In Fig. 2 we present the streamlines and the propagation of an initially flat front of tracer particles in the velocity field inside a self-affine fracture, where the flow field was averaged over the gap of the fracture. That is, velocities along and perpendicular to the mean flow direction are averaged in the z direction over the aperture of the fracture, rendering a two-dimensional (2D) flow field $\vec{u}(x,y)$. Then, using this flow field, the streamlines and the propagation of a flat front of tracer particles initially located at $x=0$ are computed. The pressure gradient, and therefore the mean flow velocity, are along the x direction, $\langle \vec{u}(x,y) \rangle = U_x \check{x}$. It can be seen that, as predicted by the effective-medium approximation, lateral fluctuations in velocity are small compared to the mean flow, and streamlines are approximately straight lines oriented along the direction of the imposed pressure difference. However, there is a substantial difference with the 2D simulations, in that in the 2D case the gap-averaged mean flow velocity is constant due to flux conservation, whereas in the 3D case, as is clear from Fig. 2, fluctuations in the gap-averaged velocity occur, and result in the broadening of the front of tracer particles as it travels through the fracture.

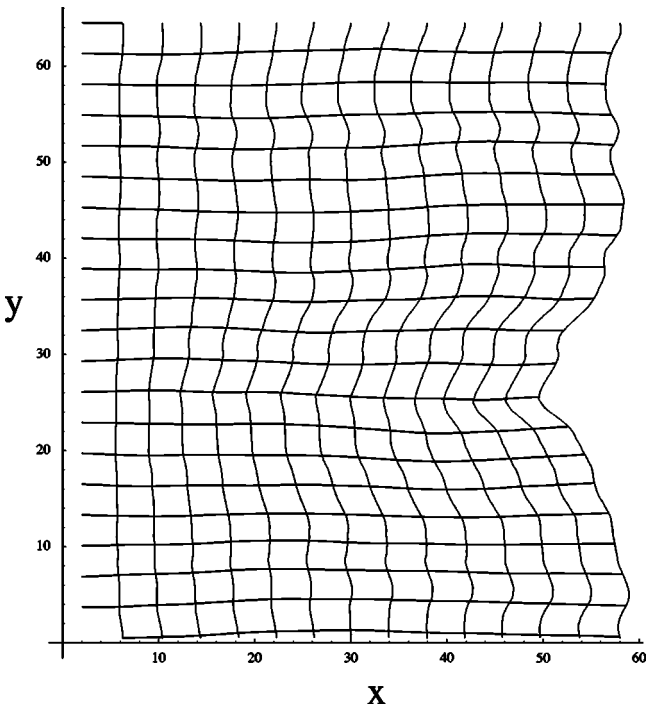

FIG. 2. Streamlines (horizontal curves) and the propagation, from left to right, of an initially flat front of tracer particles (vertical curves), injected at $x=0$, in the gap-averaged flow field. The imposed pressure drop and thus the mean flow are along the x direction. The corresponding fracture surface is shown in Fig. 1. The system size is $L=64$ and the gap between fracture surfaces is $h=8$.

C. Permeability dependence on the fracture gap

Thus far we have obtained the relation between the size of the quasilinear blocks composing our model fracture and the mean EMA conductance of the system g_m. To further obtain the dependence of g_m on the size of the fracture gap, it is first necessary to estimate the size of the unit blocks ξ in terms of h. The linear size of the unit blocks was defined as the characteristic length over which the channel formed by the two fracture surfaces can be considered, insofar as flow is concerned, as a straight one. Such an approximation is valid when the vertical fluctuations of the fracture surface over the characteristic size of a unit block are a small fraction of h. However, the size of these blocks must not be too small compared to h for the Poiseuille approximation to the flow inside the blocks to be valid. Therefore, we might expect the following relation to hold:

$$\frac{\sigma(\xi)}{h} = C_\xi \leqslant 1, \tag{13}$$

where C_ξ will be treated as a fitting parameter in our numerical simulations, and consistency with the bound (13) will be shown.

Using Eq. (2), we then obtain the small parameter ϵ in terms of h,

$$\epsilon \simeq \left[C_\xi \frac{h}{\ell}\right]^{(\zeta-1)/\zeta}. \tag{14}$$

[Note that, in the narrow fracture limit, the number of quasilinear blocks N_ξ is given by $N_\xi = (L/\xi)^2 > (L/h)^2 \gg 1$, and we can make use of the EMA results.] Inserting the previous

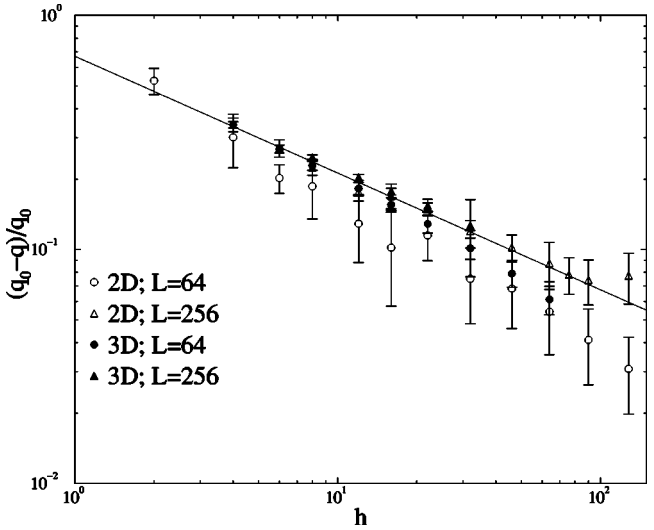

FIG. 3. Relative deviation of the flow rate per unit width from that of a straight channel as a function of the size of the vertical gap h. We compare results from 2D and 3D simulations and from two different sizes L of the system, $L=64$ and $L=256$. The solid line is a fit to the numerical results obtained in the largest 2D system.

result into Eq. (11), we obtain the dependence of the permeability of a three-dimensional self-affine fracture on the separation between surfaces,

$$k=\frac{h^2}{12}\left\{1-2\left[C_\xi\frac{h}{\ell}\right]^{2(\zeta-1)/\zeta}+5\left[C_\xi\frac{h}{\ell}\right]^{4(\zeta-1)/\zeta}+O\left(\left[C_\xi\frac{h}{\ell}\right]^{6(\zeta-1)/\zeta}\right)\right\}. \tag{15}$$

As mentioned earlier, this result is the same, through second order in ϵ, as that for two-dimensional fractures [see Eq. (33) in Ref. [7]]. In order to test this result numerically, we first recast it in terms of the flow rate per unit width q. In a straight channel of height h and length L with fixed pressure drop P, the flow rate per unit width is $q_0=h^3P/12\mu L$. In view of Eq. (15), the *relative* deviation from q_0 in a fracture of gap size h is given by

$$\frac{q_0-q}{q_0}\approx 2\left[C_\xi\frac{h}{\ell}\right]^{2(\zeta-1)/\zeta}. \tag{16}$$

In Fig. 3 we compare numerical results for the relative deviation of the flow rate per unit width from that in the parallel plate model, $(q_0-q)/q_0$, obtained in 2D and 3D fractures. In both cases, the fracture surfaces (fracture curves in the 2D case) have the same roughness exponent and the same characteristic length ℓ, and hence both have on average the same amplitude of the vertical fluctuations in surface height. We also show in Fig. 3 the scaling relation given by Eq. (16), with the value of C_ξ obtained for two-dimensional fractures in Ref. [7], $C_\xi\simeq 0.1$. As expected, C_ξ is a small number consistent with the approximation of quasilinear blocks discussed above in connection with Eq. (13). It can also be seen that, in agreement with the effective medium prediction, both 2D and 3D results are very similar. As discussed in Sec. IV B the difference between the 2D and 3D cases comes in the fourth order term, $O(\epsilon^4)$, and its correction is of relative magnitude $5\epsilon^2/2$. For the results presented in Fig. 3 the largest value of ϵ is $\epsilon\sim 0.15$ (corresponding to the smallest gap size $h=4$), hence the relative magnitude of the fourth order term is $5\epsilon^2/2\sim 0.05$, which is consistent with the observed similarity between the results obtained in 2D and 3D cases. It can also be observed that the scaling is closer to the one predicted for the large systems ($L=256$), probably due to large finite size effects present in the smaller systems.

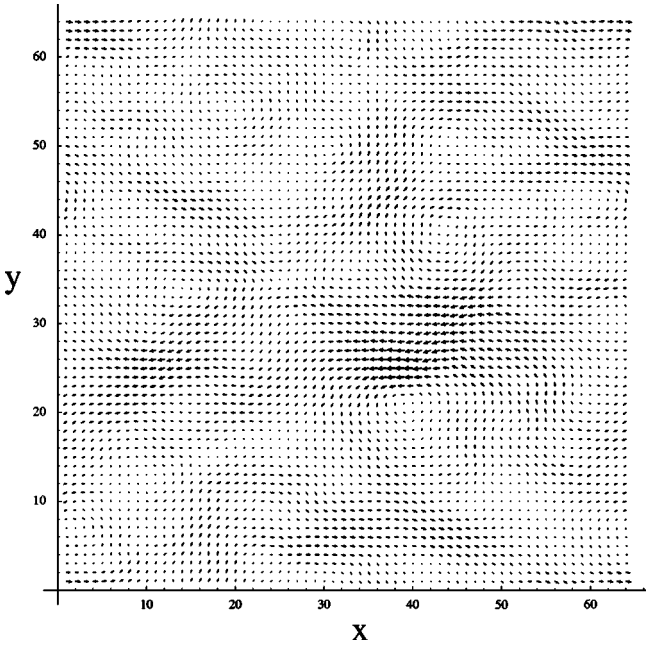

FIG. 4. Fluctuations in the gap-averaged velocity field. The fracture surface used in the numerical simulation is shown in Fig. 1, and the corresponding streamlines and front propagation are presented in Fig. 2. The size of the system is $L=64$ and the gap size is $h=8$.

D. Velocity fluctuations

In the preceding section we showed that the flow rate per unit width in 2D and 3D fractures, which have the same characteristic length ℓ, is very similar and, in fact, both have the same scaling behavior as a function of the gap size h. However, as was discussed in Sec. IV B, there is an important feature of the flow field in 3D fractures that is not present in two-dimensional simulations, that is, the presence of velocity fluctuations even after the fluid velocity is averaged over the gap of the fracture. In Fig. 4 we present the fluctuations in the gap-averaged velocity, obtained by means of the LBM in a fracture of size $L=64$ and gap size $h=8$. The corresponding fracture surface is shown in Fig. 1 and the streamlines corresponding to the gap-averaged two-dimensional velocity field are plotted in Fig. 2.

Let us then investigate the magnitude of these fluctuations in the gap-averaged velocity in the direction of the mean flow, i.e., $\delta u_x=u_x(x,y)-U_x$. Previously, in Sec. IV A, we calculated the mean EMA conductance g_m in a self-

consistent way. In a similar way, we can estimate the fluctuations in the gap-averaged velocity field in the direction of the mean flow, in terms of the variance of the extra pressure drops δp_{ab}. In fact, we might think of the random extra-pressure-drops δp_{ab} as the source of the velocity fluctuations. Let us mention that the same result would be obtained if the fluctuations are computed in terms of the variance of the induced excess of fluid flux.

The variance of the induced extra pressure drops δp_{ab} across a random bond conductance g_{ab} oriented in the direction of the flow, is given by

$$\langle \delta p^2 \rangle = (\Delta p_m)^2 \left\langle \left[\frac{g_m - g}{g_m + g} \right]^2 \right\rangle, \tag{17}$$

where Δp_m is the pressure drop in the uniform field solution, across any bond conductance oriented along the pressure difference.

Repeating now the procedure we followed to calculate the leading terms of g_m, we obtain

$$\langle \delta p^2 \rangle = \epsilon^4 (\Delta p_m)^2 \langle [x^2 - \langle x^2 \rangle]^2 \rangle. \tag{18}$$

The previous is a general result, in that it is independent of the particular distribution of heights of the fracture surface. Now, if we replace in this equation the second and fourth moments of the distribution by their normal values, $\langle x^2 \rangle = 1$ and $\langle x^4 \rangle = 3$, we obtain

$$\langle \delta p^2 \rangle = 2 \epsilon^4 (\Delta p_m)^2. \tag{19}$$

Finally, using the fact that the relative fluctuations in the pressure drop are equal to the relative fluctuations in the velocity, $\delta p / \Delta p_m = \delta u_x / U_x$, we obtain the variance in the gap-averaged velocity u_x normalized by its mean value,

$$\delta^2 \equiv \frac{\sigma_u^2}{U_x^2} = \frac{\langle \delta u_x^2 \rangle}{U_x^2} = \frac{\langle \delta p^2 \rangle}{(\Delta p_m)^2} = 2 \epsilon^4. \tag{20}$$

In order to test this result numerically, let us rewrite the previous equation in terms of the gap size h,

$$\delta = C_f \sqrt{2} \left(\frac{h}{\ell} \right)^{(2\zeta - 2)/\zeta}, \tag{21}$$

where again C_f is an adjustable parameter.

In Fig. 5 we show the numerical results obtained for the normalized fluctuations of the gap-averaged velocity in the direction of the mean flow, as a function of the distance h between unshifted fracture surfaces. We find a good agreement with the predicted exponent, that is, the fitted exponent is -0.58 ± 0.08 and the predicted one is $(2-2\zeta)/\zeta = -0.5$. The adjustable parameter is found to be $C_f = 2.1 \pm 0.9$. Note that C_ξ can be computed from C_f by means of Eq. (14), obtaining $C_\xi \simeq 0.2$, which is similar to our previous determination and is also consistent with the quasilinear approximation given by Eq. (13).

In Fig. 5 we also compare the fluctuations in the gap-averaged velocity in both directions, along and perpendicular to the mean flow. It can be observed that the scaling of the fluctuations in the velocity perpendicular to the mean flow is also given by Eq. (21), with a fitted exponent -0.6 ± 0.8. The large uncertainty in the fitted exponent comes from the fact that the fluctuations perpendicular to the mean flow have large variations between different fractures. Finally, it can be observed that fluctuations perpendicular to the mean flow are weaker than fluctuations parallel to the flow, $\delta u_x \sim 5\ \delta u_y$. The approximately constant ratio between fluctuations along and normal to the mean flow, $\delta u_x / \delta u_y \sim 5$, is consistent with the conservation of fluid flux. On the other hand, the magnitude of the velocity fluctuations are clearly related to the spatial correlations in the velocity field, and we will find an analogous asymmetry in the autocorrelation function of the velocity fluctuations. Let us mention that similar results are obtained within a macroscopic-continuum approach to the problem of transport in heterogeneous porous formations, where the magnitude of the fluctuations in the direction of the mean flow are found to be three times larger than the perpendicular ones in two-dimensional systems [39].

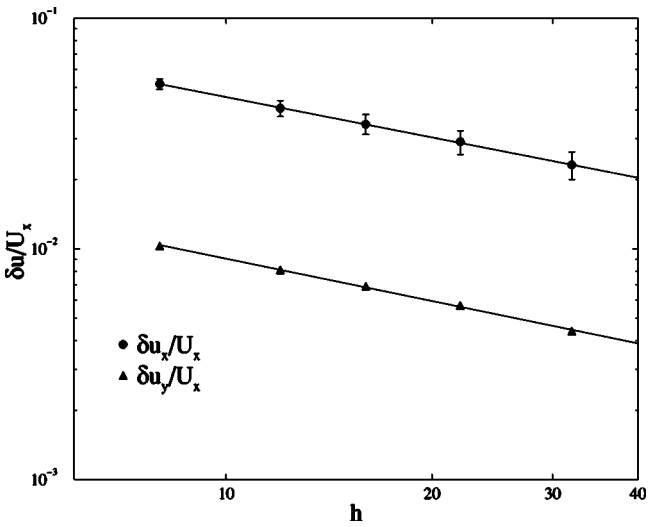

FIG. 5. Relative magnitude of the mean velocity fluctuations, both parallel and perpendicular to the mean flow, as a function of the vertical separation between surfaces h. The mean flow is in x. The size of the system is $L = 256$.

E. Fractures with shifted surfaces

Usually, when a rock is fractured its two matching surfaces are laterally shifted, that is, the displacement between them is not only vertical but also parallel to the mean plane of the fracture. We shall now consider this situation, in which the upper surface of the fracture is laterally shifted by a vector $\vec{d} = (d_\parallel, d_\perp)$ lying in the mean plane of the fracture. However, we will only consider the case where the fracture is distinctly open, that is, the two surfaces do not touch each other at any point. In this case the aperture of the fracture is no longer constant but becomes a random function of the position $a_d(x,y) = z(x + d_x, y + d_y) - z(x,y) + h$. Let us consider first, the case in which the lateral shift lies in the direction of the mean flow, i.e., $d = d_\parallel$. In Ref. [7] we investigated how such a lateral shift modifies the permeability of two-

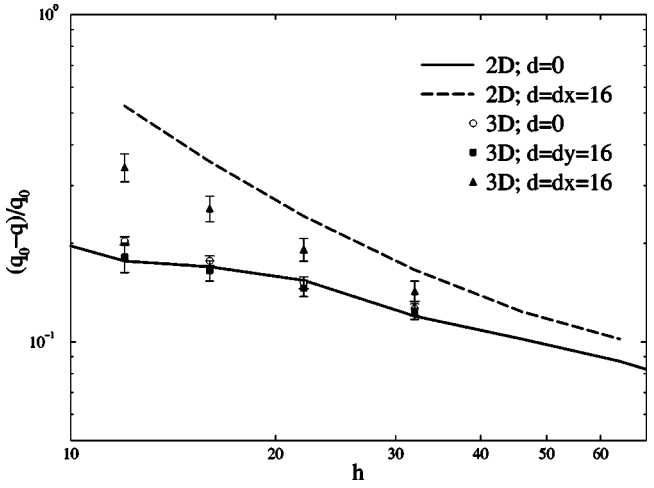

FIG. 6. Relative deviation of the flow rate per unit width from that of a straight channel, as a function of the mean vertical separation h between surfaces. The solid line corresponds to a 2D fracture formed by two complimentary surfaces that are simply displaced in the vertical direction, and the dashed line corresponds to results obtained when the upper surface of the 2D fracture is also shifted by $dx=16$ in the direction of the mean flow. Solid circles correspond to 3D simulations with no lateral shift between the matching surfaces. Open triangles and squares correspond to the upper surface shifted in the direction of the flow by $d_{\|}=16$ and perpendicular to it by $d_{\perp}=16$, respectively. The size of the system is $L=256$.

dimensional fractures. We showed that, for large separation between surfaces, such that the characteristic size ξ of the quasilinear blocks is much larger than the lateral shift $d_{\|} \ll \xi$, there is little change in the fracture geometry compared to the unshifted case, and that the permeability is asymptotically the same. On the other hand, when surfaces nearly touch at some point, the permeability will be dominated by the large pressure drop around this point, as the fluid is constrained to flow through this narrow gap. Thus, as the surfaces become closer, we found a decrease in the permeability as compared to the unshifted case. The case of three-dimensional fractures is somewhat different. For large separation between surfaces $[d_{\|} \ll \xi$; recall that $\xi=\xi(h) \propto h^{1/\zeta}]$ a behavior similar to the unshifted case is again expected, since the change in the geometry of the fracture is asymptotically negligible, and therefore, the scaling relation given by Eq. (16) should still apply. On the other hand, when surfaces are close to each other the fluid is no longer forced to flow through the narrow gaps, where the minimum separation between surfaces occur, as in the 2D case. In three dimensions, the fluid can avoid these low permeability regions by flowing around them. Thus, we might expect that the fluid rate per unit width q is bounded by the behavior in two-dimensional fractures, that is, the upper bound of q given by the two-dimensional flow rate in the case without lateral shift, and the lower-bound given by the flow rate per unit width in two-dimensional fractures with the same lateral shift, $q^{2d}_{d=d_{\|}} < q < q^{2d}_{d=0}$.

In Fig. 6 we present the relative correction to the flow rate per unit width, $(q_0-q)/q_0$, as a function of the distance

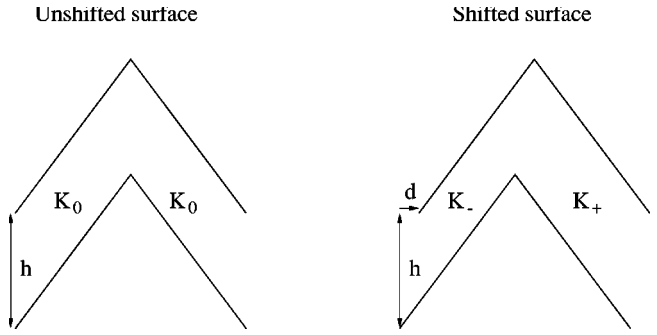

FIG. 7. Schematic representation of the intersection of a small region of the fracture with a plane containing both the displacement vector $\vec{d}$ and the normal to the fracture surfaces. The depicted region contains two consecutive quasilinear blocks of size ξ in the unshifted and shifted cases. The local permeabilities are assumed equal in the unshifted case $k=k_0$.

between surfaces, h. In agreement with our previous discussion, the correction to the flow rate obtained for three-dimensional fractures lies above the 2D case without lateral shift (upper bound for the total flow rate q) and below the two-dimensional results obtained for the same lateral shift $d=d_{\|}$ (lower bound for the total flow rate q). It can also be observed that, as we discussed earlier, for large separations between surfaces all the results converge to the unshifted situation described by Eq. (16).

In three dimensions, it is also possible to have a displacement perpendicular to the direction of the flow, $d=d_{\perp}$. Let us then investigate how the orientation of the lateral shift affects the permeability of the fracture. In Fig. 7 we show a schematic representation of the intersection of a small region of the fracture, approximated by two consecutive quasilinear blocks of size ξ, with the plane that contains both the displacement vector $\vec{d}$ and the vector normal to the mean plane of the fracture. Although extremely simplified, this schematic representation of the fracture shows the effect of the shift on the local permeability. It can be seen that, upon a lateral displacement, the unshifted local permeability of a single linear block, k_0, decreases, k_-, or increases, k_+, depending on the orientation of the quasilinear block. Specifically, an increase (decrease) in the permeability corresponds to $\theta < 0$ (>0). Furthermore, when the shift is in the direction of the flow the two channels shown in Fig. 7 will be in *series*, i.e., approximately preserving the fluid flux. On the other hand, if the shift is in the direction perpendicular to the mean flow the two blocks will be in *parallel*, that is, having approximately the same end-to-end pressure drop. It can be shown that, this somehow naive model predicts a reduction in the permeability upon a shift in the direction of the flow, and a smaller correction in the case where the shift is perpendicular to the flow, in agreement with the results presented in Fig. 6. The same effect can be observed in the experimental work reported in Ref. [5], where the flow rate was observed to be larger in the direction perpendicular to the shift between the surfaces (see Fig. 4 in Ref. [5]). It can also be observed in the experimental work presented in Ref. [5] that the difference between the flow perpendicular and parallel to the shift decreases as the separation between the

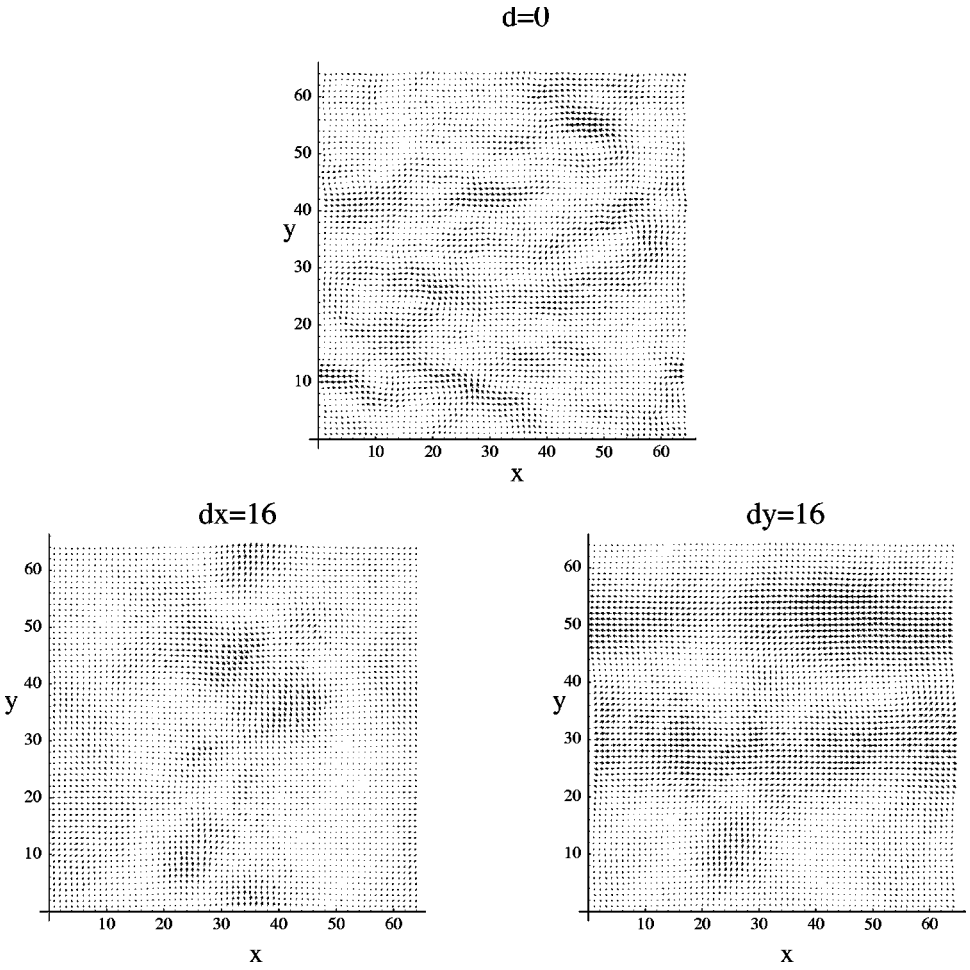

FIG. 8. The gap-averaged velocity field $\delta u(x,y)=u(x,y)-U_x\check{x}$ is presented in three different cases. On the top is the case with no lateral shift between the surfaces of the fracture. On the bottom left we show the case $d=d_{\|}=16$, and the case $d=d_{\perp}=16$ is shown on the bottom-right corner. In all cases the vertical separation between surfaces is $h=16$.

surfaces is increased, which is also in agreement with our results (see Fig. 5 in Ref. [5]). Let us mention that, in our simulations, the largest contrast between $q_{\perp}$ and $q_{\|}$, obtained for the smallest gap size $h=12$, is found to be $q_{\perp}/q_{\|}\sim 1.24$.

In Fig. 8 we show the effect of the orientation of the shift on the gap-averaged velocity fluctuations, $\delta u(x,y)=u(x,y)-U_x\check{x}$, where the mean flow is subtracted in order to magnify the fluctuations in the local velocity. The three different cases presented in Fig. 8, $d=0$, $d=d_{\|}$, and $d=d_{\perp}$, have the same vertical gap h, and correspond to the same fracture (same self-affine surface). In the case where the lateral shift is perpendicular to the flow $d=d_{\perp}$, flow channels oriented in the direction of the imposed pressure drop are apparent, whereas these oriented channels are not present when the shift is along the flow direction $d=d_{\|}$.

V. TRACER DISPERSION

Several tracer-dispersion mechanisms are present in the transport of fluids through porous media and the relative importance of these mechanisms strongly depends on the mean flow velocity [2]. Let us briefly review here the different dispersion mechanisms and their dependence on the Péclet number $\mathrm{Pe}=hU_x/D_m$, where D_m is the molecular diffusivity, h is the aperture of the fractures, and U_x is the mean flow velocity. In the case of two-dimensional fractures there are only two contributions to tracer dispersion, molecular diffusion, which dominates at very low flow rates, $\mathrm{Pe}\ll 1$, and is independent of Pe, $O(\mathrm{Pe}^0)$, and Taylor dispersion, which is $O(\mathrm{Pe}^2)$ and therefore becomes dominant at high flow rates $\mathrm{Pe}\gg 1$ [40–42]. On the other hand, in three-dimensional fractures another mechanism comes into play, that is, the presence of spatial fluctuations in the velocity field. As discussed in the preceding section, the effective aperture of the fracture is not constant, even in the case when the two complementary surfaces have no relative lateral shift, which gives rise to velocity fluctuations, as it was shown in Sec. IV D. Moreover, in contrast with the two-dimensional case, these velocity fluctuations are present even after the local velocity is averaged over the gap of the fracture. One of the main effects of the spatial fluctuations in the fluid velocity is that an initially flat invasion front of tracer particles will become increasingly distorted, resulting in its broadening in time, as it can be observed in Fig. 2. This so induced geometric dispersion of tracer particles has been reported in previous studies of dispersion in fractures [15,16] and is completely analogous to that observed in three-dimensional porous media [43]. However, let us note an important difference between previous studies and the present work. In Refs. [15,16] the analysis is based on the lubrication or Reynolds approximation, where a Poiseuille flow, with a parabolic velocity profile across the aperture, is assumed to be locally valid everywhere in the fracture. In this case, there are no

fluctuations in the local velocity in the absence of fluctuations in the local aperture of the fractures, which is in fact the case when there is no lateral shift between surfaces. On the other hand, we consider the case of narrow fractures and the lubrication approximation is not valid (at least in its simplest version). In fact, in our framework, geometric dispersion effects are present even in the absence of any lateral shift between surfaces, due to variations in the effective aperture that induce spatial fluctuations in the velocity field. This situation was investigated in recent experiments, where the broadening and dispersive behavior of an invasion front of tracer particles has been observed even in the case of no lateral shift between complementary surfaces [5].

In view of our previous discussion, we shall focus on how the fluctuations in the gap-averaged velocity affect the dispersion of the tracer particles. The molecular and Taylor contributions to the dispersion of tracer particles were discussed in our previous work, in the two-dimensional case, and they are not expected to be very sensitive to the fluctuations in the gap-averaged flow velocity, in that the molecular diffusion is clearly independent of the velocity field and the Taylor dispersion is dominated by the gradients in velocity in the direction perpendicular to the fracture surface [42]. Then, if we only account for the geometric contribution to the dispersion of tracer particles the problem can be immensely simplified. In fact, instead of working with the three-dimensional velocity field we can use the two-dimensional gap-averaged velocity field $u(x,y)$. The range in which the geometric dispersion is the dominant mechanism contributing to the dispersion of tracer particles corresponds to intermediate Péclet numbers (intermediate velocities), and the presence of such a range of Péclet numbers in self-affine fractures will be discussed in detail at the end of this section (see Sec. V C).

A. Velocity autocorrelation function

The mean-square displacement in the flow direction can be expressed in terms of the velocity autocorrelation function in time $\tilde{R}_{\|}(t)$ (Ref. [44], p. 576),

$$\begin{aligned}\langle (x-\langle x\rangle)^2\rangle_t &= 2\int_0^t d\tau\ (t-\tau)\langle [u_x(X(0),Y(0))-U_x]\\ &\quad\times[u_x(X(\tau),Y(\tau))-U_x]\rangle\\ &= 2\int_0^t d\tau\ (t-\tau)\tilde{R}_{\|}(\tau),\end{aligned} \tag{22}$$

where $x=X(t)$ and $y=Y(t)$ are the trajectories of the tracer particles incorporating the velocity fluctuations, and the average is an *ensemble* average over different realizations of the problem. Furthermore, in Sec. IV D we showed that the velocity field is approximately one dimensional, i.e., lateral fluctuations are small compared to the mean velocity ($\delta u/U_x<0.05$). The velocity autocorrelation function in time can then be related to the spatial velocity autocorrelation function, specifically to the marginal spatial autocorrelation function in the direction of the mean flow x averaged over the y direction, $R_{\|}(x)=\langle [u_x(x',y')-U_x][u_x(x'+x,y')-U_x]\rangle$, by transforming time into position through the mean flow velocity, $x=X(t)-X(0)=U_x t$. In Fig. 9 we show the equivalence between $R_{\|}$ and $\tilde{R}_{\|}$, that is, $R_{\|}(x)=\tilde{R}_{\|}(x/U_x)$. Then, we can estimate the mean-square displacement and calculate the dispersion coefficient in terms of the spatial correlation function,

$$D_H=\frac{1}{U_x}\int_0^\infty R_{\|}(\xi)\,d\xi. \tag{23}$$

From the previous equation it is clear that the dispersion coefficient depends on both the magnitude of the fluctuations and the length scale of the velocity correlations. Therefore, we introduce the characteristic correlation length of the velocity fluctuations, l_c, defined as

$$l_c=\frac{1}{\sigma_u^2}\int_0^\infty R_{\|}(x)\,dx, \tag{24}$$

where σ_u is the rms dispersion in velocity, $\sigma_u^2=\langle [u_x(x',y')-U_x]^2\rangle$. The velocity correlation length l_c measures the typical length over which fluctuations in velocity are correlated and, similarly, we can define a correlation time $\tau_c=l_c/U_x$, which measures the characteristic time scale over which fluctuations in velocity remain correlated. Let us remark that l_c is not necessarily equal to the previously defined linear size of the quasilinear blocks ξ, a fact that becomes clear upon consideration of the 2D case, where one can define a typical size ξ over which the channel formed by the opposing fracture surfaces can be considered straight, even though there are no fluctuations in the mean velocity and, therefore, the correlation length l_c cannot be defined.

In Fig. 10 we present the spatial velocity autocorrelation function in both the direction of the flow, $R_{\|}$, and perpendicular to it, $R_{\perp}$, for a system of size $L=512$ and gap size

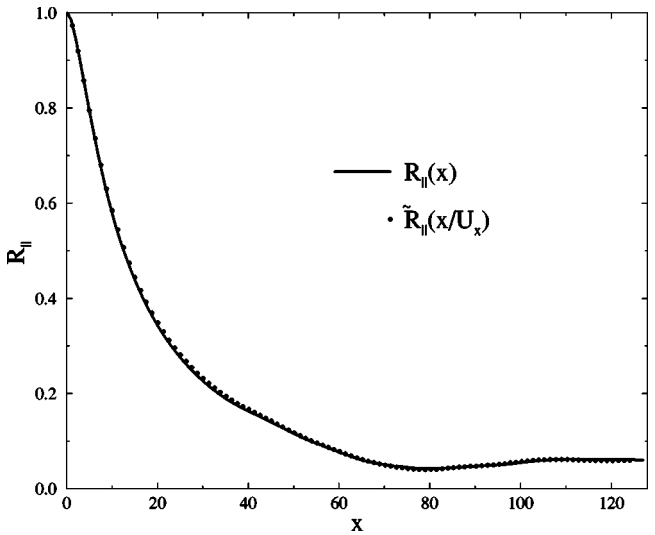

FIG. 9. Spatial velocity autocorrelation function $R_{\|}(x)$ and its comparison with $\tilde{R}_{\|}(x/U_x)$, both normalized by σ_u^2. The results correspond to a system of size $L=256$ with the fracture surfaces separated by $h=8$.

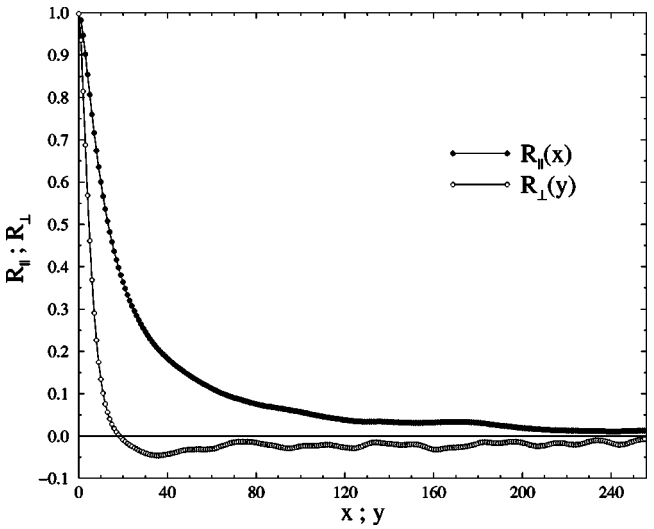

FIG. 10. Spatial velocity autocorrelation function, of the velocity component in the direction of the flow $u_x - U_x$, in both the direction of the flow $R_\parallel$ and perpendicular to it $R_\perp$. The autocorrelation functions are normalized by σ_u^2. The results correspond to a system of size $L=512$ and fracture surfaces separated by $h=8$.

$h=8$. It is clear that the spatial correlations in the direction perpendicular to the mean flow decay faster than along the flow direction, which is consistent with our previous result concerning the magnitude of the fluctuations, in that velocity fluctuations parallel to the mean flow are larger than fluctuations perpendicular to it (see Sec. IV D). It can also be observed that both correlation functions do not vanish at long distances as it should be in an infinite system. In fact, the velocity fluctuations present a positive correlation in the direction of the flow and are anticorrelated in the perpendicular direction. This nonvanishing correlation can be explained in terms of mass conservation and finite size effects. The gap-averaged velocity u_x integrated over a line perpendicular to the mean flow (from $y=0$ to $y=L$) is equal to the total flow rate Q divided by the gap size h, and it is a conserved quantity all along the system. Therefore, local fluctuations in the velocity u_x should compensate themselves, giving rise to negative spatial correlations in u_x along the direction perpendicular to the flow. This same combination of effects, that is, mass conservation and the finite size of the system, leads to the observed positive correlation in the direction of the flow. However, this nonvanishing correlation should decrease as the size of the system increases, as it can be observed in our results by comparing Fig. 9, which corresponds to a system of size $L=256$, with Fig. 10, which corresponds to $L=512$. A similar reduction of the asymptotic correlation with system size is observed in the fluctuations perpendicular to the mean flow. The negative spatial correlation in the velocity field along the direction perpendicular to the mean flow, and the fact that the velocity fluctuations decay faster in this direction, are also found in the continuum approach to transport in heterogeneous porous media [45].

B. Dependence of dispersion on the gap size

In the Stokes flow approximation ($\mathrm{Re}=0$), the flow field becomes independent of the magnitude of the flow rate, U_x being just a scaling factor [46]. Therefore, the dimensionless parameter $\delta=\sigma_u/U_x$, and the correlation length l_c, are independent of U_x. Then, rewriting Eq. (23) we obtain,

$$D_H=\delta^2 l_c U_x, \tag{25}$$

which explicitly shows the linear dependence of the dispersion coefficient on U_x. Furthermore, the dispersion of an initially flat front of tracer particles at a given distance from the injection point is independent of U_x. Consider the situation in which a front of tracer particles is injected at the inlet section of a fracture ($x=0$). The dispersion of the tracer front, measured as the mean square displacement of the tracer particles, is then given by

$$\langle (x-\langle x\rangle)^2\rangle_t = 2D_H t = 2\delta^2 l_c U_x t = 2\delta^2 l_c \langle x\rangle_t, \tag{26}$$

and it is clear that the dispersion of the front, at a fixed distance $x=\langle x\rangle$ from the inlet section $x=0$, is independent of U_x. In fact, it only depends on $l_D=\delta^2\ l_c$, where l_D is the dispersion length of the fracture [47]. This fact, that the dispersion of the front is independent of the mean flow velocity, was observed in the experiments presented in Ref. [5], where it is shown that the front shape depends on the injected volume but not on the flow rate, (see Fig. 2 in Ref. [5]).

Let us then investigate the dependence of the dispersion length l_D on the gap size h, accounting the dependence on h of both the relative magnitude of the fluctuations δ and the correlation length l_c.

The dependence of δ on the gap size was discussed in Sec. IV D, where we showed that

$$\delta^2 \propto h^{-4(1-\zeta)/\zeta}. \tag{27}$$

On the other hand, in Fig. 11 we show the correlation l_c as a function of the gap size, computed from our numerical simulations using Eq. (24), where it can be seen that the correlation length increases with the gap size h. Let us mention that, in order to minimize finite-size effects, as the previously discussed nonvanishing spatial correlations in the velocity fluctuations, present in both parallel and transverse directions, the computation of l_c was performed in the largest system we could simulate, that is, $L=1024$.

The observed decrease in the spatial correlations of the velocity field, as the surfaces become closer, might be attributed to a ''screening'' mechanism, that is, as h decreases the fluctuations in the velocity field become stronger and the velocity tends to decorrelate over a shorter distance. An analogous effect occurs in porous media flows, where a velocity disturbance from a point force decays with a characteristic ''screening'' length proportional to the square root of the permeability (as seen from the Brinkman equation [48,49]), which in our case is proportional to h (the leading order term).

As discussed earlier, the dependence of l_D on h has two opposite contributions. On one hand, the magnitude of the velocity fluctuations, δ, which decreases with increasing h and, on the other hand, the correlation length of the velocity

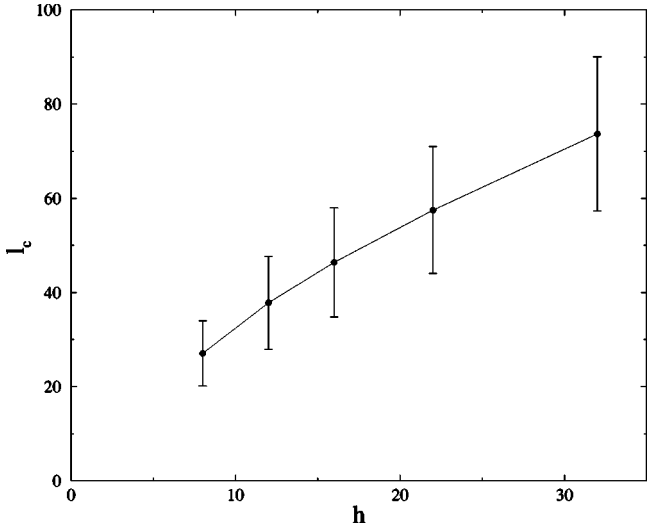

FIG. 11. Correlation length l_c as a function of the gap size h. The size of the system is $L=1024$.

fluctuations, l_c, which becomes larger as h increases. We found that, as a result of these opposite effects, the dispersion length decreases as the gap size is increased, as it can be seen in Fig. 12, where we show the dispersion length l_D as a function of the gap size h. This result is in agreement with the qualitative behavior observed in Ref. [5], where the invasion front of tracer particles becomes smoother as the gap of the fracture is increased (see Fig. 5 in Ref. [5]).

Finally, note that underlying the previous discussion is the assumption that the spatial correlations in the velocity field decay fast enough so that the integral in Eq. (23) is finite and, therefore, the broadening of the tracer front becomes diffusive at length scales larger than the correlation length l_c. Analogously, the dispersion of the front is expected to be diffusive at time scales larger than the correlation time $\tau_c = l_c/U_x$. On the other hand, in previous studies of dispersion in self-affine fractures, the slow decay in the spatial

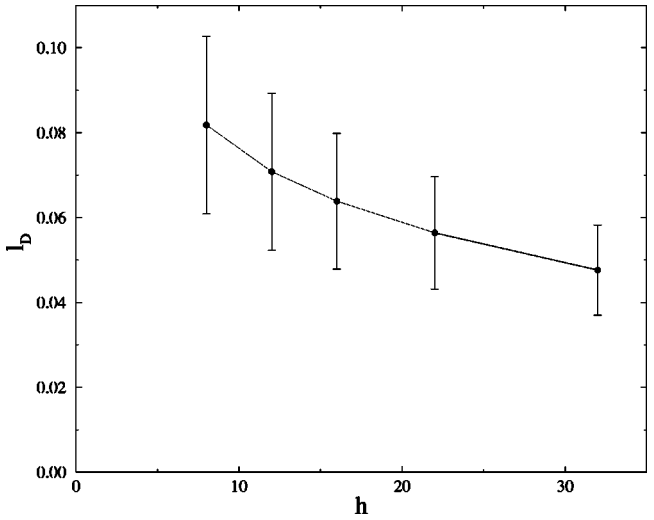

FIG. 12. Dispersion length l_D as a function of the gap size h. The size of the simulated fractures is $L=1024$.

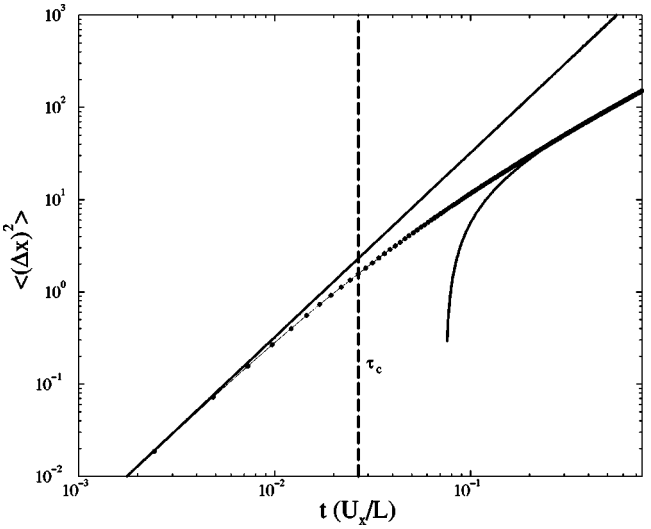

FIG. 13. Log-log plot of the mean-square displacement of an initially flat front of tracer of particles as a function of time. The vertical dashed line corresponds to the dimensionless correlation time $\tau_c = l_c/L$ above which a diffusive behavior is expected. The upper solid line corresponds to the initial highly correlated motion of the tracer particles, $\langle(\Delta x)^2\rangle = \sigma_u^2 t^2$. The lower solid line corresponds to the best fit of the linear regime, with a dispersion coefficient $D_H = (2.7 \pm 0.7) \times 10^{-5}$. [The observed departure from a linear behavior at early times is due to the constant term of the fitted linear regime, $(\Delta x)^2_{t=0} \sim -15$.] The results correspond to simulation in a system with $L=1024$ and gap size $h=8$, and were averaged over four different realizations. The time is in units of the mean transit time of the medium $T = L/U_x$.

correlations of the velocity field was proved to induce anomalous dispersion. However, those studies investigated the dispersion of tracer in the lubrication regime, where mean velocity strictly follows the fluctuations in the aperture of the fracture and long-range correlations should be expected. On the contrary, the lubrication approximation is not valid in the case of *narrow fractures*, and fluctuations in the velocity field are due mainly to the locally random orientation of the fracture channel. In Fig. 13 we present the mean square displacement of an invasion front of tracer particles as a function of time. The vertical line shows the correlation time, τ_c, after which a diffusive behavior should be expected. It can be observed that the initial behavior corresponds to the highly correlated motion of the particles and, in fact, the numerical results closely follows the solid line that is given by $\langle(\Delta x)^2\rangle = \sigma_u^2 t^2$, which is the limiting behavior of Eq. (22) for $t \to 0$. On the other hand, at times larger than τ_c the velocity begins to decorrelate from its previous values, and the dispersion of the front deviates from the quadratic behavior. Moreover, the lower solid line is given by a linear fit to the mean square displacement, in the range of times $0.2 \leqslant t U_x/L \leqslant 0.75$. The fitted value for the dispersion coefficient is $D_H = (2.7 \pm 0.7) \times 10^{-5}$, in agreement with the expected value calculated from Eq. (25), $D_H = (2.0 \pm 0.6) \times 10^{-5}$. However, the size of the system is not large enough to observe a large range where the linear, dispersive, regime is valid, and therefore the determination of the dispersion coefficient is not accurate. Nevertheless, the mean square

displacement closely follows Eq. (22) at all times and, at large enough times, it clearly grows at a much slower rate than in the anomalous regime observed in Refs. [15,16], where $(\Delta x)^2 \propto t^{2\zeta}$.

C. Tracer dispersion in the three-dimensional velocity field and tracer transit time distributions

The previous analysis of the dispersion problem was based on the assumption that the leading contribution to the dispersion of tracer particles comes from the spatial fluctuations in the gap-averaged velocity field, which allowed us to map the problem to a two-dimensional one. This approximation is only valid for values of the Péclet numbers such that both molecular and Taylor dispersion are negligible [15]. As we shall discuss, there might not be such a range of Péclet numbers, depending on the geometric properties of the fracture.

The geometric contribution to the dispersion coefficient, given by Eq. (25), is larger than the molecular diffusion term whenever the following inequality holds:

$$D_H = \delta^2 l_c U_x \gg D_m \Rightarrow \mathrm{Pe} \gg \frac{1}{\beta}, \quad \beta = \delta^2 \frac{l_c}{h}. \tag{28}$$

On the other hand, we might expect that Taylor-like dispersion becomes dominant at high flow rates, due to the presence of stagnant zones within the fracture. In that case, a heuristic estimate of the range of Péclet numbers where the geometric contribution generates a larger spreading of the tracer front than that induced by the presence of stagnant zones is given by

$$D_H = \delta^2 l_c U_x \gg D_T = \frac{h^2 U_x^2}{D_m} \Rightarrow \mathrm{Pe} \ll \beta. \tag{29}$$

Then, combining the previous two equations, it is clear that the geometric regime exists only for

$$\beta = \delta^2 \frac{l_c}{h} \gg 1. \tag{30}$$

That is, the product between the magnitude of the fluctuations in velocity and the characteristic length over which such fluctuations remain correlated should be large. Therefore, the existence of such a range of Péclet numbers in which the dispersion of tracer particles due to the velocity fluctuations is dominant, would depend on the geometrical properties of the fracture. In view of our previous results, in particular, the dependence of δ and l_c on h, we might expect that the geometric dispersion would be dominant in the limit of *narrow fractures*, i.e., large fluctuations of the surface height and small separation between fracture surfaces. In terms of the small parameter $\epsilon = \sigma_z(\xi)/\xi$, the geometric contribution will be asymptotically dominant, for any value of the Péclet number, in the limit $\epsilon \to 0$. On the other hand, as the gap of the fracture is increased, the geometric contribution will be asymptotically negligible in the limit $h \to \infty$.

Finally, let us consider the transit time distribution of tracer particles at high injection rates. Previously, we have analyzed the fully developed dispersion regime, which is valid at low injection rates or large fractures. Specifically, let us measure the transit time of tracer particles, launched at the inlet section of the fracture, that arrive at the cross section situated at a distance ΔX. If T is the mean transit time of the tracer particles, $T = \Delta X / U_x$, and τ_D is the characteristic correlation time of the tracer velocity, then the Gaussian dispersive behavior would be valid for $T \gg \tau_D$. On the other hand, when the injection rate increases and the transit time becomes $T \lesssim \tau_D$, the transit time distribution deviates from a Gaussian distributions and exponential tails are generally observed in flow through porous media [15,50,51].

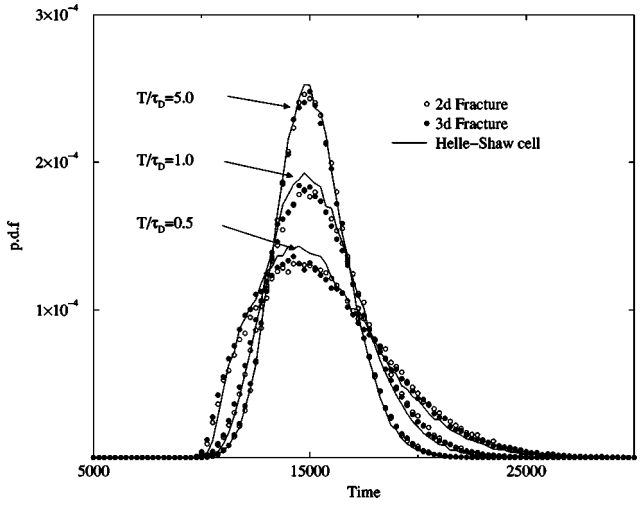

FIG. 14. Transit time distribution of tracer particles for three different ratios between the transit and correlation times, $T/\tau_D = 1/2$, 1, and 5.0, and for three different systems, a Hele-Shaw cell, 2D and 3D fractures. The simulation correspond to a system of size $L = 512$, gap size $h = 16$ and the transit time distributions are measured at a distance $\Delta X = 400$ from the injection point.

In the flow through fractures, as well as in the flow in a Hele-Shaw cell, the correlation time of the velocity is given by the diffusive time across the gap. For transit times $T \lesssim \tau_D$ the tracer particles do not have time to diffuse across the gap and their velocity will remain correlated during their convective motion throughout the system. In this case, stagnant or low-velocity zones have the effect of retarding the tracer particles, and give rise to the exponential tails, due to the fact that diffusive motion is the only mechanism available for the particles to leave these stagnant zones [52]. In Fig. 14 we present the tracer transit time distribution for three different ratios between the transit and the correlation times, $T/\tau_D = 1/2$, 1, and 5.0, and for three different systems, Hele-Shaw cells, 2D and 3D fractures. First of all, it can be observed that, for $T/\tau_D \gg 1$, all the transit time distributions are Gaussian and very similar to each other. On the other hand, as the transit times becomes $T/\tau_D \lesssim 1$, the distributions deviate from a Gaussian curve, becoming increasingly asymmetric. It can also be observed that both two- and three-dimensional fractures present slightly more persistent tails than in the Hele-Shaw case. The similarity between the distribution in 2D and 3D fractures is in total agreement with our previous results, where the velocity field for three-

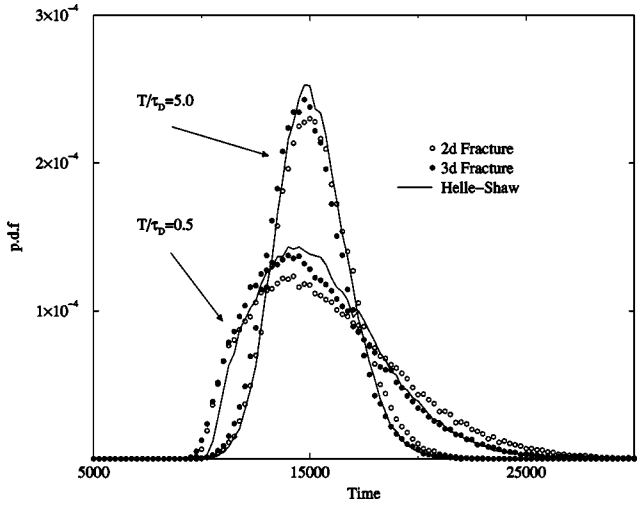

FIG. 15. Transit time distribution of tracer particles for two different ratios between the transit and correlation times, $T/\tau_D = 1/2$ and 5.0, and for three different systems, a Hele-Shaw cell, 2D and 3D fractures with opposite surfaces laterally displaced by $d = dx = 16$. The simulation corresponds to a system of size $L = 512$, gap size $h = 16$ and the transit time distributions are measured at a distance $\Delta X = 400$ from the injection point.

dimensional fractures was shown to be quasi-two-dimensional in the absence of a lateral shift between the surfaces of the fracture. On the other hand, we feel that the small difference between the transit time distribution in self-affine fractures and in the Hele-Shaw cell might be related to the presence of low-velocity zones in the fractures, which are not present in a straight channel. This enhancement of the long-time tails due to the presence of low-velocity zones should be more evident in the presence of a lateral shift.

In Fig. 15 we present the transit time distribution of tracer particles, in the same three different cases as in Fig. 14, but in this case the upper surface of the fractures is laterally shifted in the direction of the flow by $d = dx = 16$. First of all, it can be observed that, as in the unshifted case presented in Fig. 14, all distributions are Gaussian and very similar to each other for large transit times, $T/\tau_D = 5.0$. On the other hand, for much smaller transit times, $T/\tau_D = 0.2$, a long-time tail develops, in particular in the case of two-dimensional fractures. As shown in Sec. IV E, two-dimensional fractures present lower permeabilities than the three-dimensional ones in the presence of a lateral shift, due to the fact that in the 3D case the fluid can avoid low permeability regions by flowing around them. Therefore, the presence of low-velocity zones is more important in 2D and thereby the effect of these zones on the long-time behavior of the transit time distribution becomes more important.

VI. SUMMARY AND CONCLUSIONS

Transport properties of three-dimensional self-affine rough fractures were investigated by means of the effective-medium approximation and numerical simulations using the Lattice-Boltzmann method. The numerical simulations verified the scaling behavior predicted by the effective-medium approach and, furthermore, allowed us to compute important transport parameters of the fractures, such as the dispersion length, and their dependence on the aperture. Two different cases were investigated, the unshifted case, in which the two matching surfaces of the fracture are displaced in the direction normal to the mean plane, and the shifted one, in which the upper surface is laterally displaced either in the direction of the flow or perpendicular to it.

First, we modeled the fractures by a regular two-dimensional square lattice of bond conductances, and the lattice spacing and the distribution of bond conductivities were related to the geometrical properties of the fracture. Specifically, we related the lattice spacing to the length scale over which fluctuations in the surface height are small compared to the aperture of the fracture, and it was determined in terms of the roughness exponent, the characteristic length and the aperture of the fractures. Then, adapting some well-known results obtained by means of the effective-medium approximation in the analogous random-resistor network, we obtained the permeability of the fracture and its dependence on the aperture in the limit of *narrow fractures*. We showed that the permeability is, up to second order in a perturbative parameter, the same as in two-dimensional fractures. This quasi-two-dimensional behavior of the transport of fluids through self-affine fractures was confirmed by the numerical computations of the streamlines, which presented very small lateral fluctuations. A similar behavior was also observed in the experimental work reported in Ref. [5], in that the structure developed by the invasion front of tracer particles presents very small fluctuations perpendicular to the mean flow in the unshifted case [see Fig. 4(a) in Ref. [5]]. Moreover, the scaling behavior of the permeability with the aperture was verified by our numerical results and, in addition to that, we showed that it is in agreement with numerical results performed in two-dimensional fractures. However, we also discussed an important difference between the 3D and 2D cases, namely, the presence of fluctuations in the gap-averaged fluid velocity in three-dimensional fractures, and we were further able to predict the scaling behavior of the velocity fluctuations in the direction of the mean flow by means of the effective-medium approximation. The numerical simulations were in agreement with this result and, furthermore, showed that the velocity fluctuations in the direction perpendicular to the flow have the same scaling but are approximately three times smaller in magnitude. Similar results were obtained in the continuum approach to transport in heterogeneous porous media [39,45]. Finally, we investigated the case of shifted surfaces and showed that the permeability of the fractures strongly depends on the orientation of the shift, which is either in the direction of the imposed pressure drop or perpendicular to it, in the limit of *narrow fractures*. Furthermore, by means of numerical simulations we showed that the flow rate per unit width in three-dimensional fractures is bounded by the two-dimensional results. Specifically, for a relative shift in the direction perpendicular to the mean flow the permeability is slightly affected and lies above the permeability of two-dimensional fractures. On the other hand, when the upper surface is shifted in the direction of the flow the permeability is largely reduced, but not as much as in the

two-dimensional case. The latter is due to the fact that in three-dimensional fractures, in contrast with the two-dimensional case, the fluid can avoid low-permeability regions by flowing around them. We also presented a simplified representation of a local region of the fracture that, although naive in character, captures the effect of the orientation of the shift on the permeability of the fracture. The same effect is observed in experiments, in that the flow rate is larger in the direction perpendicular to the relative shift between surfaces (see Fig. 4 in Ref. [5]).

In the second part of this work, we investigated the dispersion of tracer particles in self-affine fractures. Specifically, we analyzed the dependence of the geometric contribution to the dispersion process on the aperture of the fracture. First, we simplified the analysis by mapping the problem to the dispersion of tracer particles in the two-dimensional gap-averaged velocity field. We then distinguished between the two contributions to the dispersion coefficient, namely, the relative magnitude of the velocity fluctuations and their correlation length. We observed that, in agreement with previous studies [39,45], the autocorrelation function of the velocity fluctuations decays faster in the direction perpendicular to the mean flow. Finally, we showed that, even though the correlation length increases with the aperture, the dispersion coefficient is asymptotically small in the limit of wide fractures. The latter effect is also observed in the experiments presented in Ref. [5] where it was shown that the invasion front of tracer particles becomes increasingly smooth as the aperture of the fracture is increased.

Finally, we investigated the dispersion of tracer particles in the fully three-dimensional velocity field inside the fractures. Specifically, we discussed the range of Péclet numbers in which the geometric contribution to dispersion is expected to be dominant and we showed that, depending on the geometric properties of the fracture, there might be no such range of Péclet numbers. However, we found that the geometric dispersion is dominant in the limit of *narrow fractures*, and in general is dominant for dispersion lengths larger than the aperture of the fractures. We also investigated the transit time distribution of tracer particles, and their dependence on the mean transit time. We showed that, as the mean transit time is reduced and it becomes comparable to or smaller than the correlation time of the tracer velocity, the transit time distribution becomes increasingly non-Gaussian, developing long-time tails due to the presence of low-velocity zones where the only mechanism for tracer transport is molecular diffusion. In general, the transit time distributions are very similar to the case of tracer dispersion in a Hele-Shaw cell, except for the case of two-dimensional fractures shifted in the direction of the flow, which present the largest tails probably due to an enhancement of the low-velocity zones by the relative shift between surfaces. In fact, in agreement with the latter results, the two-dimensional fractures, with the upper surface shifted in the direction of the flow, were shown to have the lowest permeability.

ACKNOWLEDGMENTS

We thank J. P. Hulin and H. Auradou for useful discussions and for sharing with us their experimental results; G. Dagan for carefully reading the manuscript and for his many suggestions; R. Chertcoff, I. Ippolito, D. L. Johnson, and N. Nerone for useful discussions. This research was supported by the Geosciences Research Program, Office of Basic Energy Sciences, U.S. Department of Energy, and computational facilities were provided by the National Energy Resources Scientific Computer Center. G.D. thanks Conicet Argentina and the University of Buenos Aires for partial support.

[1] J. Bear, *Dynamics of Fluids in Porous Media* (Elsevier, New York, 1972).
[2] F.A.L. Dullien, *Porous Media. Fluid Transport and Pore Structure*, 2nd ed. (Academic Press, New York, 1991).
[3] M. Sahimi, *Flow and Transport in Porous Media and Fractured Rock* (VCH, Weinheim, 1995).
[4] P. Dijk and B. Berkowitz, Water Resour. Res. **35**, 3955 (1999).
[5] H. Auradou, J.P. Hulin, and S. Roux, Phys. Rev. E **63**, 066306 (2001).
[6] S.R. Brown, J. Geophys. Res. **92**, 1337 (1987).
[7] G. Drazer and J. Koplik, Phys. Rev. E **62**, 8076 (2000).
[8] E. Bouchaud, G. Lapasset, and J. Planès, Europhys. Lett. **13**, 73 (1990).
[9] F. Plouraboué, P. Kurowski, J.-P. Hulin, S. Roux, and J. Schmittbuhl, Phys. Rev. E **51**, 1675 (1995).
[10] F. Plouraboué, K.W. Winkler, L. Petitjean, J.-P. Hulin, and S. Roux, Phys. Rev. E **53**, 277 (1996).
[11] Y. Méheust and J. Schmittbuhl, Geophys. Res. Lett. **27**, 2989 (2000).
[12] Y.W. Tsang, Water Resour. Res. **20**, 1209 (1984).
[13] S.R. Brown, J. Geophys. Res. **94**, 9429 (1989).
[14] J.B. Walsh, S.R. Brown, and W.B. Durham, J. Geophys. Res. **102**, 22 587 (1997).
[15] F. Plouraboué, J.-P. Hulin, S. Roux, and J. Koplik, Phys. Rev. E **58**, 3334 (1998).
[16] S. Roux, F. Plouraboué, and J.P. Hulin, Transp. Porous Media **32**, 97 (1998).
[17] Y. Meheust and J. Schmittbuhl, J. Geophys. Res. **106**, 2089 (2001).
[18] A.P. Oron and B. Berkowitz, Water Resour. Res. **34**, 2811 (1998).
[19] B.B. Mandelbrot, *The Fractal Geometry of Nature* (Freeman, New York, 1983).
[20] S.R. Brown and C.H. Scholz, J. Geophys. Res. **90**, 12 575 (1985).
[21] C.Y. Poon, R.S. Sayles, and T.A. Jones, J. Phys. D **25**, 1269 (1992).
[22] J. Schmittbuhl, S. Gentier, and S. Roux, Geophys. Res. Lett. **20**, 639 (1993).
[23] W.L. Power and W.B. Durham, Int. J. Rock Mech. Min. Sci. **34**, 979 (1997).
[24] J. Feder, *Fractals* (Plenum Press, New York, 1988).

[25] J. Boffa, C. Allain, and J.P. Hulin, Physica A **278**, 65 (2000).
[26] R.F. Voss, *Fundamental Algorithms in Computer Graphics* (Springer-Verlag, Berlin, 1985), pp. 805–835.
[27] J. Kondev, C.L. Henley, and D.G. Salinas, Phys. Rev. E **61**, 104 (2000).
[28] D.H. Rothman and S. Zaleski, *Lattice-Gas Cellular Automata* (Cambridge University Press, Cambridge, 1997).
[29] D.A. Wolf-Gladrow, *Lattice-Gas Cellular Automata and Lattice Boltzmann Models*, Lecture Notes in Mathematics Vol. 1725 (Springer-Verlag, Berlin, 2000).
[30] E. Skjetne, A. Hansen, and J.S. Gudmundsson, J. Fluid Mech. **383**, 1 (1999).
[31] S. Kirkpatrick, Rev. Mod. Phys. **45**, 574 (1973).
[32] J. Koplik, in *Physics of Granular Media*, edited by D. Bideau and J. Dodds (Nova Science, New York, 1991), p. 215.
[33] P.M. Adler and B. Berkowitz, Transp. Porous Media **40**, 145 (2000).
[34] J. Koplik, J. Fluid Mech. **119**, 219 (1982).
[35] M. Sahimi, Rev. Mod. Phys. **65**, 1393 (1993).
[36] J. Koplik, J. Phys. C **14**, 4821 (1981).
[37] V.V. Mourzenko, J.-F. Thovert, and P.M. Adler, Phys. Rev. E **53**, 5606 (1996).
[38] J.M. Luck, Phys. Rev. B **43**, 3933 (1991).
[39] G. Dagan, J. Fluid Mech. **145**, 151 (1984).
[40] J. Koplik, I. Ippolito, and J.P. Hulin, Phys. Fluids A **5**, 1333 (1993).
[41] R. Gutfraind, I. Ippolito, and A. Hansen, Phys. Fluids **7**, 1938 (1995).
[42] G. Drazer and J. Koplik, Phys. Rev. E **63**, 056104 (2001).
[43] P.G. Saffman, J. Fluid Mech. **6**, 321 (1959).
[44] F. Reif, *Fundamentals of Statistical and Thermal Physics* (McGraw-Hill, London, 1965).
[45] G. Dagan, *Flow and Transport in Porous Formations* (Springer-Verlag, New York, 1989).
[46] G.K. Batchelor, *An Introduction to Fluid Dynamics* (Cambridge University Press, New York, 1999).
[47] J.C. Bacri, N. Rakotomalala, and D. Salin, Phys. Rev. Lett. **58**, 2035 (1987).
[48] H.C. Brinkman, Appl. Sci. Res., Sect. A **1**, 27 (1947).
[49] L. Durlofsky, J.F. Brady, and G. Bossis, J. Fluid Mech. **180**, 21 (1987).
[50] K.H. Coats and B.D. Smith, Soc. Pet. Eng. J. **231**, 73 (1964).
[51] G. Drazer, R. Chertcoff, L. Bruno, M. Rosen, and J.P. Hulin, Chem. Eng. Sci. **54**, 4137 (1999).
[52] J.P. Bouchaud and A. Georges, Phys. Rep. **195**, 127 (1990).